

# On the size-dependent phase transformation in nanoparticulate zirconia

Tomas Chraska <sup>a</sup>, Alexander H. King <sup>b,\*</sup>, Christopher C. Berndt <sup>c</sup>

<sup>a</sup> Department of Materials Science and Engineering, University of Virginia, Charlottesville, VA 22903-2442, USA

<sup>b</sup> School of Materials Engineering, Purdue University, West Lafayette, IN 47907-1289, USA

<sup>c</sup> Department of Materials Science and Engineering, State University of New York at Stony Brook, Stony Brook, NY 11794-2275, USA

## Abstract

We have studied the structures of zirconia nanoparticles formed by plasma-spraying an organo-metallic precursor. Inspection of the particles in the TEM reveals that they adopt one of two distinct crystal structures, depending upon their size. The smallest particles have the tetragonal structure, while larger ones are monoclinic. Interpolation of the data reveals a critical size above which the monoclinic structure is stable. Upon annealing, the zirconia particles coarsen and undergo a phase transformation when the particle size is of the order of 18 nm, for reasons associated with the surface energy, and the occurrence of this phase transformation produces a sudden change in the driving force for coarsening. Grain size distributions below the critical size for the transformation are log-normal, but as the transformation occurs, the size distribution changes to a markedly less skewed form. The development of this distribution is followed to establish whether it grows self-similarly, or returns to log-normality once normal driving forces are restored after the phase transformation is complete. © 2000 Elsevier Science S.A. All rights reserved.

**Keywords:** Zirconia; Nanoparticles; Phase stability; Coarsening; Particle size distribution; Surface energy

## 1. Introduction

Zirconia has become one of the most industrially important ceramic materials of the present time. The traditional applications of  $ZrO_2$  and  $ZrO_2$ -containing materials are foundry sands and flours, refractory ceramic, and abrasives. Due to its high oxygen ion conduction and high refractive index, it is also used in a wide range of newer applications which include catalysts, oxygen sensors, fuel cells, and jewelry. Since the publication of the famous paper on 'ceramic steel' (transformation toughened zirconia) by Garvie et al. [1], zirconias have also been utilized in many mechanical applications. Along with high strength and toughness, zirconia also possesses good hardness, wear resistance, and thermal shock resistance. These properties have led to the use of zirconia-based components in a number of engineering applications such as automobile engine parts, wire drawing dies and cutting tools.

The low thermal conductivity together with relatively high coefficient of thermal expansion makes zirconia a suitable material for thermal barrier coatings on metal components.

At atmospheric pressure, zirconia exists in three crystalline polymorphs namely cubic, tetragonal, and monoclinic. The stable polymorph at room temperature and atmospheric pressure of pure coarse grained zirconia is monoclinic (Space group  $P2_1/c$ ) which transforms martensitically at 1170°C to tetragonal ( $P4_2/nmc$ ) and then at 2370°C to a fluorite-type ( $Fm\bar{3}m$ ) cubic structure [2,3].

At high pressures three slightly different orthorhombic polymorphs have been reported [4,5]. The mechanism of the cubic to tetragonal phase transformation has not been studied in pure  $ZrO_2$ , but occurs in a displacive but nonmartensitic fashion in cubic alloys of the  $ZrO_2$ - $Y_2O_3$  system [6,7]. The martensitic transformation from the tetragonal to monoclinic structure has great importance for mechanical applications since it is the basis for transformation toughening.

The high temperature polymorphs of pure zirconia cannot be retained by quenching to room temperature

\* Corresponding author. Tel.: +1-765-4944100; fax: +1-765-4941204.

E-mail address: alexking@ecn.purdue.edu (A.H. King)

[3]. Stabilizers such as  $Y_2O_3$ ,  $MgO$ ,  $CaO$  are commonly added to zirconia to promote the retention of the high temperature polymorphs. Depending on the amount of stabilizer and on a particular heat treatment regime, three forms of stabilized zirconias can be achieved. [6,8], fully stabilized zirconia (FSZ) which contains only the cubic polymorph, partially stabilized zirconia (PSZ) containing fine ( $\sim 0.2$   $\mu m$ ) tetragonal particles in a cubic matrix, and finally so called tetragonal zirconia polycrystals (TZP) which comprises only fine ( $\sim 0.4$   $\mu m$ ) grains of the tetragonal crystal structure. Another way of stabilizing the high temperature tetragonal phase of pure zirconia at room temperature is to reduce the particle or grain size into the nanometer regime [9,10].

In this paper, we consider why a high temperature polymorph is found to be stable in as prepared nanocrystalline zirconia particles which are smaller than a certain critical size. Secondly, annealing experiments resulting in coarsening are presented and the consequent phase transformation and its influence on the particle size distribution character are discussed.

## 2. Experimental procedures

Nanocrystalline powders of pure  $ZrO_2$  were prepared by liquid thermal spray synthesis [11]. A conventional atmospheric plasma spray torch (Miller Thermal SG 100) was modified to incorporate a special liquid injector in place of the usual powder injection port and tube, and used to produce the high temperature plasma jet. The injector, which works on the two-fluid atomization principle with nitrogen as the atomizing gas, produces atomized droplets of the liquid organo-metallic precursor and injects it into the high pressure plume of the plasma jet. An electrostatic precipitator (ESP) consisting of a pair of polished stainless steel plates (100 x 100 x 2 mm) separated by a 10 mm thick ceramic insulator is placed parallel to the trajectory of the spray jet (Fig. 1). An electric field of  $6 \text{ kV cm}^{-1}$  was applied in the ESP so that the spray particles could be collected on the plates by electrophoresis (Fig. 1). The electrostatic precipitator can be replaced by just one polished

steel substrate which is placed perpendicular to the trajectory of the spray beam.

A volume of 20 ml of 80 wt.% zirconium butoxide in n-butanol was diluted with 300 ml of n-butanol to obtain the 2.4 wt.% zirconia liquid precursor. The liquid feed rate was maintained at  $6.8 \text{ ml min}^{-1}$ . The stand-off distance of both the ESP plate edge or the substrate from the torch nozzle was maintained on 100 mm.

The collected powder was then annealed at 500 or 900°C for 1 or 2 h in air and slowly cooled down in the furnace. Both annealing temperatures are set below the first transformation temperature for coarse-grained  $ZrO_2$  [12].

Small quantities (0.001 g) of the collected and annealed powders were dispersed ultrasonically in propanol and then allowed to settle on carbon coated copper grids for investigation by transmission electron microscopy (TEM). TEM investigations were performed at 120 kV in a Philips CM 12 or at 200 kV in a Philips CM 200 FEG. Bright field and dark field imaging were used to study the particle size and size distribution. The chemistry of powder specimens was established in TEM by energy dispersive X-ray spectroscopy (EDS). The phase composition of the powder specimens was established by X-ray diffraction (XRD) with Cu-K $\alpha$  radiation and by selected area electron diffraction SAED.

XRD line profile analysis was carried out to estimate the average particle size using integral breadth analysis [13]. The applicability of this method for loose nanocrystalline powder samples was recently confirmed by Jiang et al. [14]. Assuming that the overall broadening of XRD lines is comprised of two effects: one arising from the small coherent grain size and the other from the atomic level strain (microstrain), the extraction of grain size and microstrain requires the separation of these two components. The integral peak width resulting from a small grain size effect alone can be well described by the Scherrer equation. The integral width resulting from microstrain alone may be expressed as:

$$\delta 2\theta = 4\varepsilon \tan \theta \quad (1)$$

where  $\delta 2\theta$  is the integral width of XRD lines in radians and  $\varepsilon$  is the microstrain. Both theoretical and experimental work tend to show that strain broadening may be closely approximated by a Gaussian function, whereas the effects of small crystalline size more closely resemble a Cauchy broadening profile. When both effects are responsible for peak broadening, the combined relation may be arranged in the form

$$\frac{(\delta 2\theta)^2}{\tan^2 \theta_0} = \frac{K\lambda}{D} \left( \frac{\delta 2\theta}{\tan \theta_0 \sin \theta_0} \right) + 16\varepsilon^2 \quad (2)$$

where  $\theta_0$  is the position of the peak maximum, and  $K$  is a constant (usually set to unity [13]). By plotting

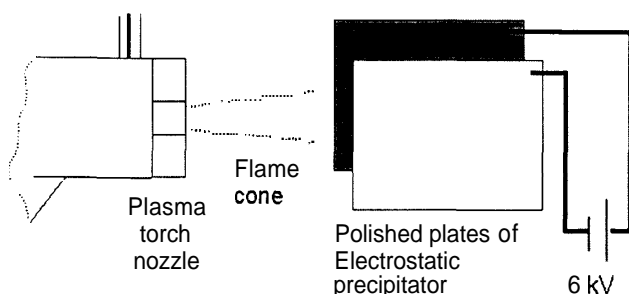


Fig. 1. Schematic drawing of the electrostatic precipitator.

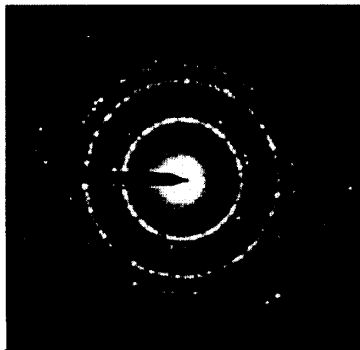
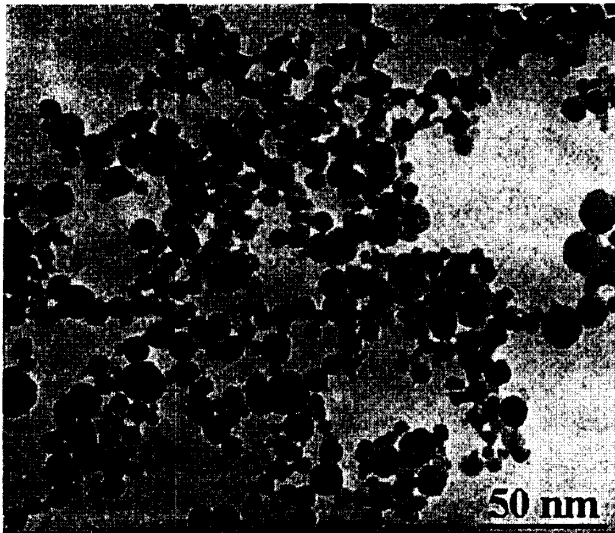


Fig. 2. (a) Bright-field TEM image of tetragonal zirconia nanoparticles collected by ESP; (b) corresponding selected area diffraction pattern.

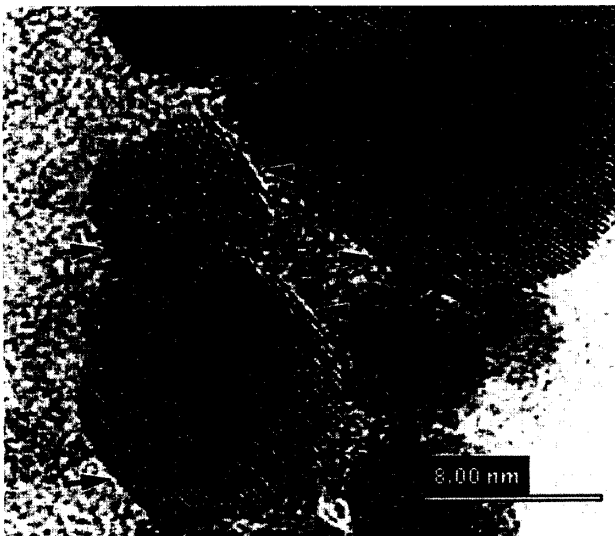


Fig. 3. High-resolution electron micrograph of tetragonal zirconia nanoparticles. Arrows point to the  $\{111\}$  facets.

$(62\theta)^2/(\tan^2\theta_0)$  against  $(62\theta)/(\tan\theta_0\sin\theta_0)$  from few broadened XRD lines one can obtain the slope,  $K\lambda/D$ , and extract the average grain size  $D$ . An XRD spectrum of a standard silica specimen was used to measure the instrumental broadening. Contributions due to  $K\alpha_1$  and  $K\alpha_2$  were deconvoluted in the XRD line profile fitting program that was used to determine the peak positions and their integral width. A computer program (UnitCell 2.1) was used to calculate corresponding lattice parameters by the least square fitting method.

TEM images were digitized and analyzed by image analysis program NIH Image (version 1.61) on a computer. Individual particles were manually encircled and a computer routine measured the corresponding perimeters. The mean particle sizes given in this chapter are mean equivalent cylindrical diameters obtained from the measured particle perimeters of more than 300 particles in each case.

### 3. Experimental results

#### 3.1. As-prepared nanocrystalline zirconia particles

The EDS confirms that only zirconium is present in as-prepared powders collected on the ESP (our X-ray detector is not capable of detecting oxygen). The XRD spectra of the powder show only the lines of tetragonal zirconia phase. This result suggests that the necessary physical and chemical processes [11] have been completed in the plasma jet and the liquid feedstock has transformed into tetragonal zirconia particles. The diffraction lines are broad, indicating that the powder is made of very fine particles.

Typical TEM bright field (BF) images of zirconia powder are shown in Fig. 2a. These TEM images show single, partially overlapping, equiaxed nanocrystalline particles with no indication of defects such as dislocations, twins, etc. Although the particles are touching each other they only rarely exhibit connecting necks. Particle sizes range from 2 to 14 nm. A typical selected area diffraction pattern of these particles (Fig. 2b) exhibits a spotty ring structure, which is produced by fine tetragonal zirconia particles. Conical dark field imaging showed that the ring structure was formed by the fine particles and that all the particles are crystalline. High resolution images confirmed that only small number of particles exhibits facets. If a particle is faceted then it is mostly parallel to the  $\{111\}$  plane, as shown in Fig. 3.

The average grain size of as-prepared nanoparticles; as determined from XRD line broadening was 5.6 nm. The grain size distribution shown in Fig. 4, determined from bright-field and dark-field TEM images of more than 300 particles, is log-normal. The average grain size is 5.5 nm (standard deviation (SD)  $a = 2.1$ ) which is in

excellent agreement with the XRD result. Log-normality was confirmed by both Kolmogorov–Smirnov and  $\chi^2$  tests when the normality hypothesis was rejected at

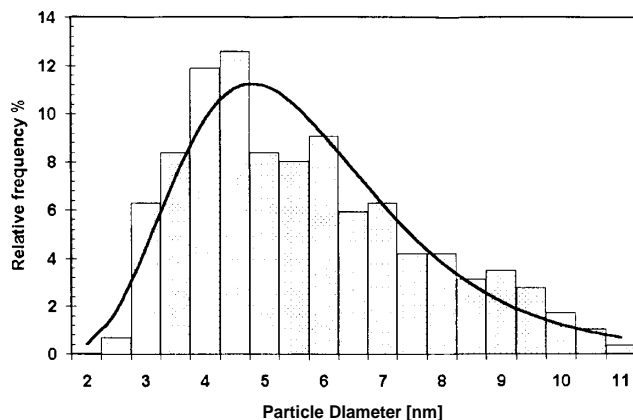


Fig. 4. Histogram of the particle size distribution of as-prepared zirconia nanoparticles collected by ESP, and a fitted log-normal distribution function.

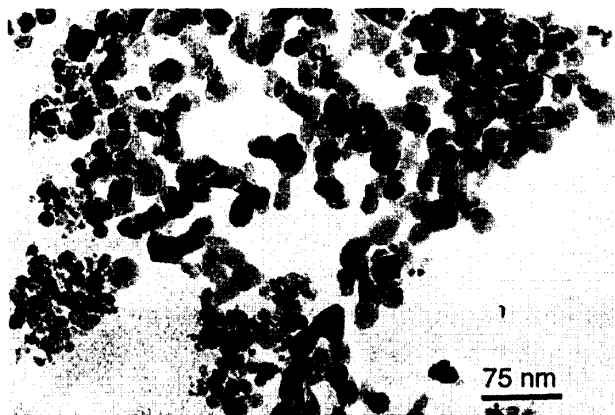


Fig. 5. TEM bright-field image of zirconia powder collected on a substrate. Both tetragonal (*t*) and monoclinic (*m*) phases are present.

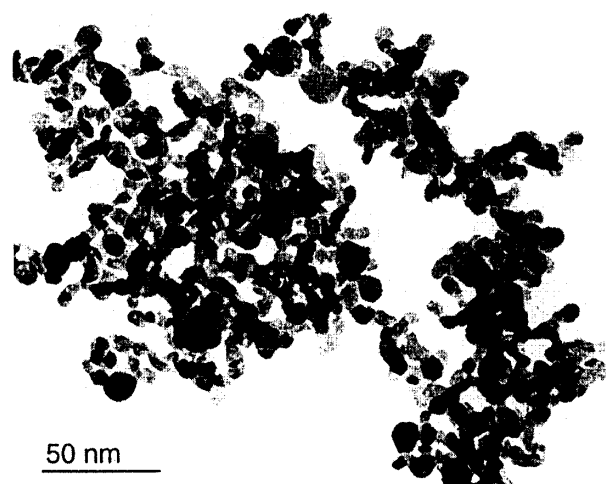


Fig. 6. TEM bright-field image of zirconia powder after annealing at 500°C for 1 h.

a significance level  $\alpha = 5\%$  whereas the log-normality hypothesis could not be rejected even at higher  $\alpha$ .

The XRD spectra of powder collected on a substrate perpendicular to the trajectory of the spray beam show that both tetragonal and monoclinic zirconia phases are present. Two types of particles can be seen in a bright field TEM image (Fig. 5) ranging from 3 to 70 nm. Bigger and rather oblong particles are monoclinic zirconia as identified from the appropriate SAED pattern and smaller circular particles are tetragonal zirconia. The average particle size of monoclinic zirconia is 22 nm as determined from the TEM micrographs. For tetragonal zirconia, the average size is 10.5 nm (from TEM) which is only slightly greater than the size of ESP-collected tetragonal particles and suggests that there is a critical particle size above which the monoclinic structure becomes stable.

### 3.2. Annealing of nanocrystalline zirconia particles

A small quantity of as-sprayed powder was annealed at 500°C for 1 h in air. The XRD spectra of the annealed powder correspond to the tetragonal phase but two small peaks, which are the two strongest lines of the monoclinic phase, were also present. The relative abundance of monoclinic phase is less than 5% as determined from the relative XRD line intensities by the polymorph method [5]. A typical TEM bright field image of annealed zirconia nanoparticles is shown in Fig. 6, well distinguishable though many of them are connected by necks and therefore being somewhat elongated. Particle sizes range from 5 to 18 nm. Particle coarsening occurred during the annealing, as can be further seen from the grain size distribution (Fig. 7) which is also log-normal. The normality hypothesis was rejected by the Kolmogorov–Smirnov test and by the  $\chi^2$  test tests at a significance level  $\alpha = 10\%$ . The log-normal hypothesis could not be rejected even at  $\alpha = 15\%$ . The average grain size calculated from line broadening was 9.5 nm, and measured from TEM images it was 9.9 nm ( $\sigma = 2.2$ ).

Annealing at 900°C for 1 h results in more pronounced particle coarsening and extensive phase transformation to the monoclinic phase. Approximately 70% of the zirconia powder transformed to the monoclinic polymorph and the remaining 30% was tetragonal, as determined from the relative XRD line intensities [5]. Both polymorphs can be recognized in the TEM image (Fig. 8). There are no distinct defect features inside the particles except strain contours in some monoclinic particles. The monoclinic particles are substantially larger than the tetragonal ones and are no longer equiaxed but rather elongated as they grow and form necks (Fig. 9) upon contact with each other. Many of the *m* grains exhibit preferably  $(\bar{1}11)$  facets (Fig. 10). The sintering process (growing of necks) is much faster

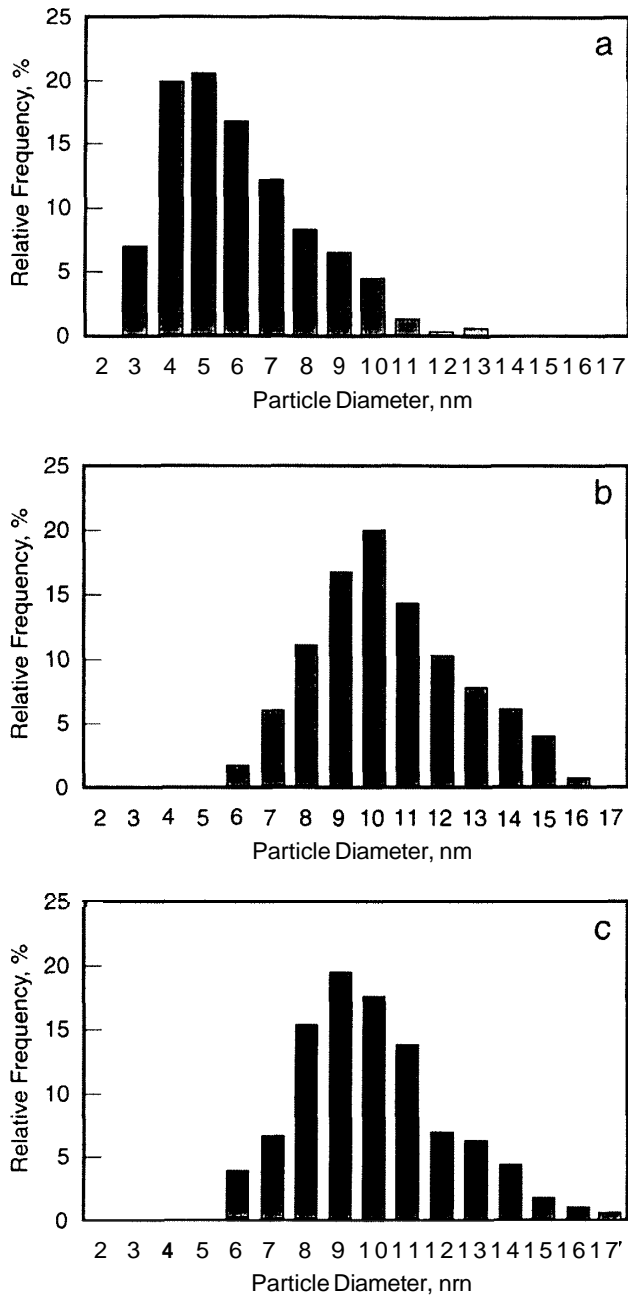


Fig. 7. Particle size distributions of nanocrystalline tetragonal zirconia: (a) as prepared; (b) after annealing at 500°C for 1 h; (c) after annealing at 900°C for 1 h.

for the monoclinic particles since the tetragonal particles remain near-equiaxed with only minor necks developed. This indicates that the surface energy to grain boundary energy ratio is considerably greater for monoclinic nanoparticles; and favors grain boundaries over the free surface. Some of the touching tetragonal nanoparticles formed a single grain during the annealing (Fig. 10) suggesting that the nanoparticles are unconstrained, and able to rotate and find the minimum intergranular energy. (In-situ observations of this rotation phenomenon during the sintering of n-ZrO<sub>2</sub>, have

been reported by Rankin et al. [15]) The particle surfaces are, therefore, free of impurities or adsorbed molecules as proved by the formation of clean grain boundaries (Fig. 9) or by the occurrence of particle rotation (Fig. 11).

The grain size distribution of the tetragonal particles after 900°C/1 h annealing (Fig. 7c) is again log-normal with the average size being 9.5 nm ( $\sigma = 2.3$ ) and maximum particle size below 20 nm. Normality hypothesis was rejected by the Kolmogorov–Smirnov test at a significance level  $\alpha = 5\%$  and by the  $\chi^2$  test tests at a significance level  $\alpha = 10\%$ . The log-normal hypothesis could not be rejected even at higher  $\alpha$ . The average, the SD, and the maximum particle size of tetragonal nanoparticles after 900°C/1 h annealing are basically the same as are the ones after 500°C/1 h annealing. The

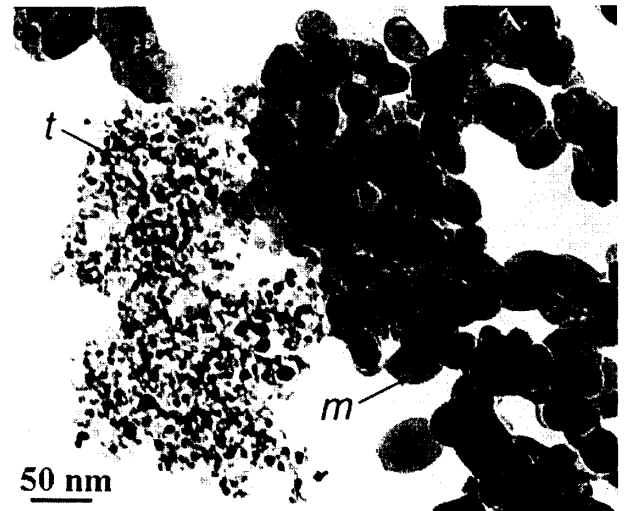


Fig. 8. TEM bright-field image of zirconia powder after annealing at 900°C for 1 h. Both tetragonal (t) and monoclinic (m) phases are present.

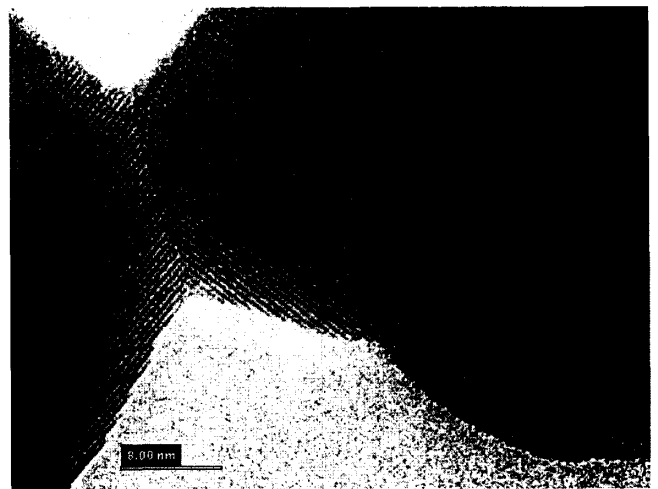


Fig. 9. High resolution TEM image of a neck and grain boundary between two monoclinic particles.

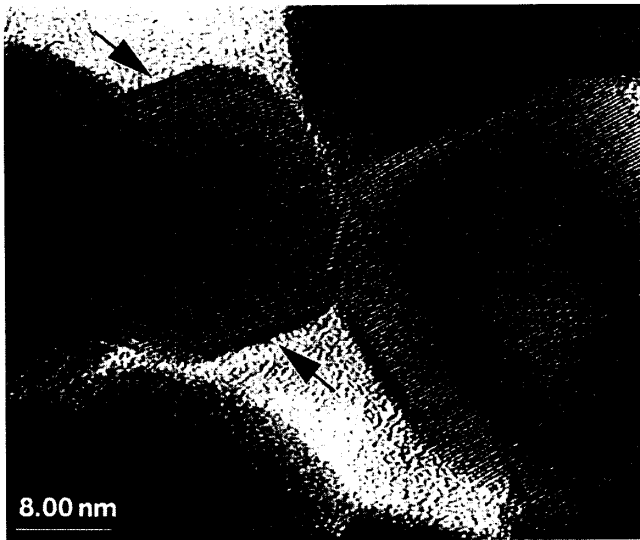


Fig. 10. High resolution TEM image of monoclinic particles showing (111) facets (marked with arrows).

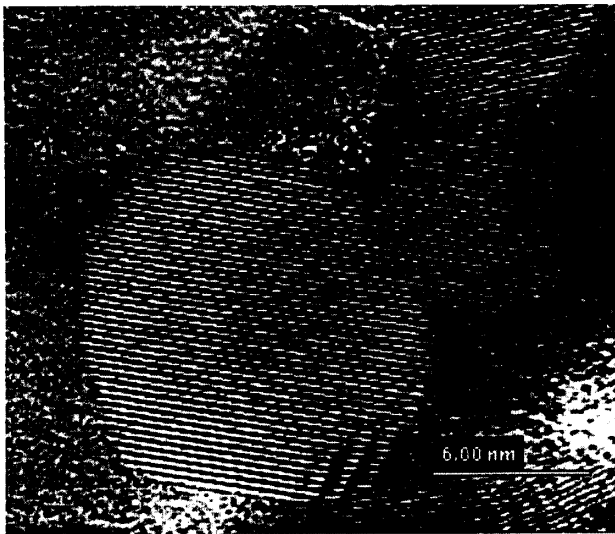


Fig. 11. HRTEM image of two tetragonal nanoparticles (A and B) forming a single grain.

tetragonal nanoparticle populations in both annealed samples have the same log-normal distribution even though the relative abundance of tetragonal particles in the whole sample is diminishing with increased annealing temperature. The average size of the monoclinic grains is 40.3 nm ( $\sigma = 9.5$ ) and the grain size distribution is shown in Fig. 12a. The log-normal distribution hypothesis can be rejected at significance level  $\alpha = 20\%$  using Kohnogorov–Sinirnov test and at significance level  $\alpha = 15\%$  using  $\chi^2$  test whereas the normal distribution hypothesis cannot be rejected by either of the tests.

After annealing at 900°C for 2 h all nanoparticles have transformed to monoclinic phase with no tetragonal zirconia particles remaining. Further particle coarsening and sintering resulted in defect formation (e.g.

stacking faults) which can be seen in Fig. 13. Some of the grains are faceted and almost all of them have created grain boundaries with neighboring grains. The average grain size is 137 nm ( $\sigma = 36$ ) and grain size distribution is shown in Fig. 12b. Using the Kolmogorov–Smirnov test, the log-normal distribution hy-

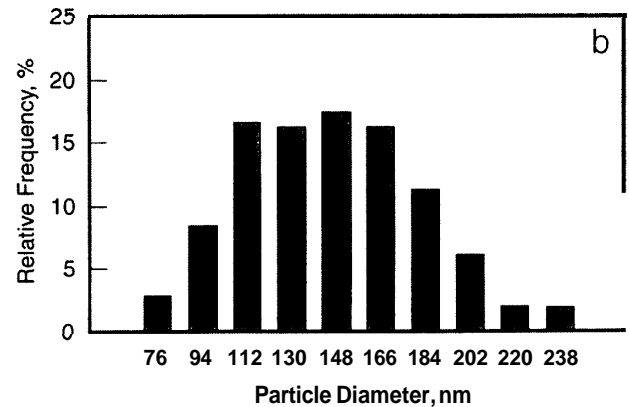
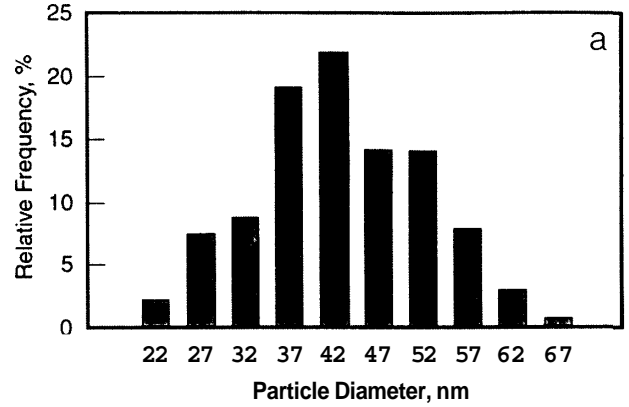


Fig. 12. Particle size distributions of nanocrystalline monoclinic zirconia: (a) after annealing at 900°C for 1 h; (b) after annealing at 900°C for 2 h.

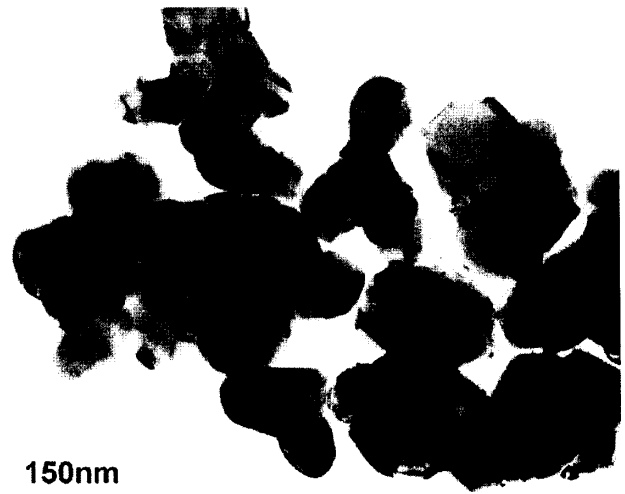


Fig. 13. TEM bright-field image of monoclinic zirconia particles after annealing at 900°C for 2 h.

hypothesis can be rejected at significance level  $\alpha = 10\%$  whereas the normal distribution hypothesis cannot be rejected. Using  $\chi^2$  tests, the log-normal distribution hypothesis can be rejected at significance level  $\alpha = 15\%$  whereas the normal distribution hypothesis cannot be rejected by either of the tests.

## 4. Discussion

### 4.1. Stability of tetragonal zirconia particles

The tetragonal zirconia nanoparticles coarsen upon annealing. From the presented results, one can conclude that any coarsening above a certain critical size results in particle transformation to the monoclinic phase. The critical size, up to which the tetragonal phase is stable, is around 18 nm in diameter (9 nm radius).

Various explanations have been proposed for the observed stabilization of high temperature tetragonal (t) phase in nanocrystalline zirconia particles at room temperature and controversies still exist in the elucidation of the mechanism of the t-phase stability. Garvie proposed that the lower surface energy of the tetragonal  $\text{ZrO}_2$  was the cause for this phase to be present in nanocrystalline form at or below room temperature [10,16,17]. He predicted that particles below about 10 nm in diameter are stabilized in the tetragonal form, and those that are above this critical particle size are subject to the  $t \rightarrow$  monoclinic (m) transformation.

Later, Murase and Kato suggested that water vapor increased the rate of crystallite growth and decreased surface energy having thus significant effect on the  $t \rightarrow$  m transformation [18]. Domain boundaries were also suggested to inhibit the  $t \rightarrow$  m transformation thus leading to tetragonal phase stability [19]. Osendi et al. postulated that the initial nucleation of  $t\text{-ZrO}_2$  is favored by anionic vacancies with trapped electrons [20]. Tani et al. proposed a mechanism of topotactic crystallization of  $t\text{-ZrO}_2$  on nuclei in the amorphous  $\text{ZrO}_2$  [21]. Recently, Srinivasan et al. argued against the concept proposed Garvie (stabilization due to lower surface energy of the t phase) as they found monoclinic particles with much smaller diameters [22]. They suggested that anionic oxygen vacancies present on the surface control the  $t \rightarrow$  m phase transformation on cooling, and that oxygen adsorption triggers this phase transformation. All the articles cited here, except the one by Garvie [10], have in common that the zirconia nanoparticles were produced by various chemical methods (precipitation and calcination). Chemical factors such as adsorbed atoms and purity of raw materials play important roles in the stability of nanocrystalline zirconia and they may completely alter the original surface energy consideration. Therefore, none of the

above explanations have a general validity for pure nanocrystalline zirconia.

One of the most recent explanations is based on increased effective internal pressure due to surface curvature and small particle radius (the Gibbs-Thomson effect):

$$\Delta p = 2\gamma/r \quad (3)$$

where  $\Delta p$  is the difference between external and internal pressure,  $\gamma$  is the surface energy, and  $r$  is the particle radius. Skandan et al. first proposed that the increased internal pressure at small radii was responsible for the stability of the high-pressure polymorph of yttria in nanocrystalline grains [9]. This explanation has been since then quite often used for several nanocrystalline ceramic systems (e.g.  $\text{Y}_2\text{O}_3$  [23],  $\text{TiO}_2$  [24]), as the stabilization of high-temperature or high-pressure polymorph in nanoparticles appeared to be a more general phenomenon. The concept of stabilization by internal pressure has been used extensively in the work of Nitsche et al. [25–28] and Skandan [29,30], for the case of nanocrystalline zirconia prepared by the inert gas condensation technique. This method of preparing nano- $\text{ZrO}_2$  provides high purity powders and compacts.

The phase determination of the zirconia nanocrystals remains somewhat ambiguous too. Some authors, using Rietveld analysis of XRD spectra, described the phase as the high-pressure tetragonal phase [29,30], which is in fact found to be orthorhombic. In situ high pressure neutron diffraction measurement of coarse grained zirconia made clear that what was previously called the high-pressure tetragonal phase [31] has orthorhombic (Pbca) symmetry [4,32]. Others, also using Rietveld analysis, confirmed that the phase of  $n\text{-ZrO}_2$  particles below a critical size is the high temperature modification (P42/nmc) [25,27]. The critical size was estimated to be between 8 and 12 nm in diameter. It was pointed out, however, that even the Rietveld analysis is not able to distinguish unambiguously between the orthorhombic and tetragonal polymorphs. The differences in the lattice parameters and in the lattice symmetries of the two modifications are too small to be detected by XRD even for coarse grained zirconia [4,32]. This problem is further complicated in the case of nanocrystals by pronounced line broadening due to the very small crystallite size.

In the present work, the XRD spectra of as-prepared and 500°C/1 h annealed powders were indexed as the high temperature tetragonal polymorph (P42/nmc). XRD line positions obtained from the fitting procedure were used to calculate corresponding lattice parameters by the least square fitting procedure. The results are presented in Table 1.

The room temperature lattice parameters for pure tetragonal zirconia were obtained by extrapolating high temperature neutron data for pure coarse grained zirco-

Table 1  
Comparison of measured and anticipated lattice parameters for tetragonal zirconia<sup>a</sup>

	Lattice parameters (nm)	
	<i>a</i>	<i>c</i>
As-prepared nanocrystalline <i>t</i> -ZrO <sub>2</sub>	0.50813 ± 0.00044	0.51989 ± 0.00039
Annealed nanocrystalline <i>t</i> -ZrO <sub>2</sub>	0.50781 ± 0.00045	0.51968 ± 0.00048
Extrapolated to room temperature from data for bulk, high-temperature <i>t</i> -ZrO <sub>2</sub> , at one atmosphere [12]	0.50832	0.51993
Hypothetical values at room temperature, under 3 GPa pressure	0.50542	0.51705

<sup>a</sup>The lattice parameters in the nanoparticles match the data for bulk *t*-ZrO<sub>2</sub> at one atmosphere, within the experimental error. They are clearly distinguishable from the expected values under the hypothesized internal pressure.

nia [12] using the linear expansion coefficient. The lattice parameters thus obtained are in excellent agreement with those measured from our nanocrystalline zirconia. In other words, the lattice parameters of the zirconia nanocrystals at room temperature are the same as would be those of coarse grained pure tetragonal zirconia at room temperature. This result casts some doubts on the concept of increase internal pressure in nanoparticles. If we take as the value of internal pressure  $A_p = 3$  GPa (suggested by Winterer et al. [27] for 8 nm particles) and calculate corresponding strains with the help of theoretical single crystal elastic constants [33,34] we can also calculate the corresponding hypothetical lattice parameters under this pressure. As one can see from Table 1, the hypothetical parameters are significantly smaller than both the experimental ones of *n*-ZrO<sub>2</sub> and those of coarse grained tetragonal ZrO<sub>2</sub> extrapolated to room temperature. In other words, if the zirconia nanoparticles were really under hydrostatic pressure as large as 3 GPa we should observe an XRD line position shift. The line shift would be easily distinguishable especially at higher Bragg angles, despite the pronounced line broadening. Therefore this experiment calls into question the plausibility the Gibbs-Thompson effect as an explanation of the tetragonal phase stability in zirconia nanocrystals. Further, the postulated hydrostatic pressure of 3 GPa corresponds to a surface stress of approximately  $5 \text{ N m}^{-1}$  at a diameter of 6 nm: this value appears unphysically large, when compared with a surface energy typically of the order of  $1 \text{ J m}^{-2}$ .

The only remaining explanation is the one originally suggested by Garvie [10,16]. In this simple thermody-

namical approach, the free energy of an unconstrained spherical particle,  $G$ , may be expressed as

$$G = \frac{4}{3}\pi r^3 \cdot G_V + 4\pi r^2 \cdot \gamma \quad (4)$$

where  $r$  is the radius of a particle,  $G_V$  is the free energy per unit volume of an infinite crystal, and  $\gamma$  is the surface energy of the crystal. The difference in free energy of the two polymorphs is then given by

$$\Delta G(r) = \frac{4}{3}\pi r^3 \cdot \Delta G_V + 4\pi r^2 \cdot (\gamma_t - \gamma_m) \quad (5)$$

where the  $\Delta G_V$  is the free energy difference for the phase transition per unit volume of an infinite crystal. Assuming that the *t* phase has lower surface energy than the *m* phase, if we now reduce the particle size to some critical value,  $r_c$ , where  $\Delta G(r_c)$  is 0 at some temperature,  $T$  below the normal transformation temperature, the high temperature *t* form can exist and one can write the critical radius as

$$r_c = \frac{-3(\gamma_t - \gamma_m)}{AH(1 - T/T_b)} \quad (6)$$

where  $AH$  is the heat of transformation per unit volume of an infinite crystal, and  $T_b$  the transformation temperature of an infinite crystal. Using  $\gamma_t = 0.77 \text{ J m}^{-2}$ ,  $\gamma_m = 1.13 \text{ J m}^{-2}$ , and  $AH = 2.82 \times 10^8 \text{ J m}^{-3}$  (all being determined from calorimetry) and  $T_b = 1175^\circ\text{C}$  in Eq. (6), Garvie has estimated the critical radius  $r_c$  to be 5 nm [16,17].

A recent first-principle study of zirconia surfaces concludes that the  $(\bar{1}11)$  and  $(111)$  faces are the most stable surfaces of the *m* and *t* phases, respectively, and also that the surface energy is considerably anisotropic [35]. The observed  $(\bar{1}11)$  and  $(111)$  facets in the *m* (Fig. 10) and *t* (Fig. 3) phases, respectively, support this calculation. The surface energy of the most stable monoclinic and tetragonal surfaces are, however, equal ( $1.24 \text{ J m}^{-2}$  at 0 K), to within the accuracy of the calculation accuracy. This result is inconsistent with the assumption of Eq. (6) that the surface energy of *t* phase is lower than that of *m* phase. This contradiction can, however, be reconciled. It is well established that a definite orientation relationship exists between crystalline directions upon the *t* → *m* transformation. It is found that  $(100)_m \parallel (100)_t$  and  $[001]_m \parallel [001]_t$  ( $T < 1000^\circ\text{C}$ ). Due to this orientation relationship, upon the *t* → *m* martensitic transformation we obtain

$$\{111\}_t \rightarrow \begin{cases} \{\bar{1}11\}_m \\ \{111\}_m \end{cases}$$

in equal amounts. The  $\{111\}_m$  faces are less stable having higher surface energy ( $1.54 \text{ J m}^{-2}$  at 0 K). Therefore, the orientational constraint on the *t* → *m* martensitic transformation forces some favorable *t* surfaces to turn into unfavorable *m* surfaces, which inhibits the transformation.

For a quantitative estimate of  $r_c$  it is necessary to calculate room temperature values of the surface energy by including the surface entropy of *t*- and *m*-ZrO<sub>2</sub>. The surface entropy of *t*-ZrO<sub>2</sub> is of order 0.4 mJ m<sup>-2</sup> K<sup>-1</sup>) [36]. The surface entropy of *m*-ZrO<sub>2</sub> was set to 0.2 mJ m<sup>-2</sup> K<sup>-1</sup>) according to the expectation expressed in [35]. Eq. (6) gives then a value of about 7 nm for the critical radius, which is closer to the observed value than the one suggested by Garvie [10]. In practice, the surface entropies used here are only estimates, and the resulting surface energies apply only to a portion of the surface of the particles, making the precise application of Eq. (6) rather a wishful task. It is clear, however, that the room-temperature stability of tetragonal *n*-ZrO<sub>2</sub> results from differences of surface energy between the *m* and *t* phases, rather than a stabilizing internal pressure.

#### 4.2. Particle size distributions

The production of zirconia nanocrystalline powder by the liquid thermal spray synthesis (LTSS) gives results that are very similar to those obtained for powder prepared by the inert gas condensation method. Both powders are chemically very clean and the achievable size range and size distribution are almost the same. LTSS has the advantage of a considerably higher powder production rate [11].

The *t* → *m* transformation, discussed above, produces a step-function change in the driving force for coarsening, which provides an interesting experimental opportunity. Structural scale variations, either in polycrystals or powders, usually approximate log-normal distributions and coarsening produces a self-similar shift in the distribution as smaller particles (or grains) are absorbed by larger ones (except in the case of abnormal grain growth). In the process of normal grain growth or particle coarsening, then, the log-normal size distribution persists through the development of the structure. It is postulated that any size distribution will coarsen in a self-similar manner, and this is known as the 'statistical self-similarity' (SSS) hypothesis [37]. There is, however, very little detailed experimental evidence to support the SSS hypothesis for differing size distributions.

All of the particle size distributions below the critical size for the tetragonal to monoclinic phase transformation in our experiment, are log-normal. All the grain size distributions above the critical point were more normal-like. The change in the shape of the distribution is evidently associated with the phase transformation, and more specifically with a corresponding change in coarsening rate. From the results in this work, it is suggested that the coarsening rate for the monoclinic particles is markedly faster than for the tetragonal particles that they replace. The driving force for coarsening

is proportional to the surface energy, so a transformation to a phase of higher surface energy should increase the particle coarsening rate, if all other parameters are unchanged. This has the effect of shifting the peak of the distribution to the right, as transforming particles accelerate their growth, while the untransformed particles continue to grow only slowly making the distribution becomes more symmetrical and normal-like.

Further coarsening of the normally-distributed monoclinic grains is found here to occur in a self-similar manner, with no distinguishable change in the shape of the distribution. There is no apparent tendency, at the relatively short times of our studies, to return to a log-normal distribution. This leads us to conclude that log-normal distributions are not intrinsically preferred. Particle coarsening before and after the transformation is self-similar.

It remains unclear whether self-similar coarsening will occur for any size distribution, or only for certain special cases. One might conceive of experiments in which square-shaped distributions are created, and it might be expected that the sharp cut-offs would be softened by the particle coarsening process. It would be interesting, for such a case, to see whether the symmetry of the distribution were maintained in such a change.

## 5. Conclusions

Pure tetragonal nanoparticulate zirconia transforms to the monoclinic structure at a critical radius of approximately 9 nm.

The stability of the tetragonal phase in nanoparticulate zirconia derives from the lower surface energy of that phase, which dominates the free energy at small particle sizes, and not from the internal pressure of the particles.

The particle sizes in the tetragonal phase are well characterized by a log-normal distribution. In the monoclinic phase, however, the distribution is more normal-like.

Particle coarsening follows the statistical self-similarity hypothesis for both the log-normally distributed *t*-ZrO<sub>2</sub> particles and the normally-distributed *m*-ZrO<sub>2</sub>.

## Acknowledgements

We are grateful to Dr J. Karthikeyan for assistance in producing the specimens. This work was supported by the National Science Foundation through grant number CTS-9312896; and also through the Center for Thermal Spray Research, MRSEC program grant number DMR-9632570.

## References

- [1] R.C. Garvie, R.H. Hannink, R.T. Pascoe, *Nature* 258 (1975) 703.
- [2] M. Ruehle, *Adv. Mater.* 9 (1997) 195.
- [3] E.C. Subbarao, in: A.H. Heuer, L.W. Hobbs (Eds.), *Advances in Ceramics-Science and Technology of Zirconia*, American Ceramic Society, 1981, p. 1.
- [4] J.M. Leger, P.E. Tomaszewski, A. Atouf, A.S. Pereira, *Phys. Rev. B* 47 (1993) 75.
- [5] C.J. Howard, R.J. Hill, *J. Mater. Sci.* 26 (1991) 127.
- [6] A.H. Heuer, *J. Am. Ceram. Soc.* 70 (1987) 689.
- [7] A.H. Heuer, R. Chaim, V. Lanteri, *Acta Metall.* 35 (1987) 661.
- [8] F. Kroupa, *Czechoslov. J. Phys. A* 37 (1987) 552.
- [9] G. Skandan, C.M. Foster, H. Frase, M.N. Ali, J.C. Parker, H. Hahn, *Nanostruct. Mater.* 1 (1992) 313.
- [10] R.C. Garvie, M.F. Goss, *J. Mater. Sci.* 21 (1986) 1253.
- [11] J. Karthikeyan, C.C. Berndt, J. Tikkanen, J.Y. Wang, A.H. King, H. Herman, *Nanostruct. Mater.* 8 (1997) 61.
- [12] H. Boysen, F. Frey, T. Vogt, *Acta Crystallogr. B* 47 (1991) 881.
- [13] H.P. Klug, L.E. Alexander, *X-ray Diffraction Procedures for Polycrystalline and Amorphous Materials*, Wiley, New York, 1974.
- [14] H.G. Jiang, M. Ruehle, E.J. Lavemia, *J. Mater. Res.* 14 (1999) 549.
- [15] J. Rankin, B.W. Sheldon, *Mater. Sci. Eng. A* 204 (1995) 48.
- [16] R.C. Garvie, *J. Phys. Chem.* 69 (1965) 1298.
- [17] R.C. Garvie, *J. Phys. Chem.* 82 (1978) 218.
- [18] J. Murase, J. Kato, *J. Am. Ceram. Soc.* 66 (1982) 196.
- [19] T. Mitsuhashi, M. Ichihata, U. Tatsuke, *J. Am. Ceram. Soc.* 67 (1974) 97.
- [20] M.I. Osendi, J.S. Moya, C.J. Serna, J. Soria, *J. Am. Ceram. Soc.* 68 (1985) 135.
- [21] E. Tani, M. Yoshimura, S. Somiya, *J. Am. Ceram. Soc.* 66 (1985) 11.
- [22] R. Srinivasan, L. Rice, B.H. Davis, *J. Am. Ceram. Soc.* 68 (1990) 135.
- [23] H. Hahn, *Nanostruct. Mater.* 2 (1993) 251.
- [24] H. Zhang, J.F. Banfield, in: E. Ma, P. Bellon, M. Atzmon, R. Trivedi (Eds.), *Phase Transformations in Systems Driven Far From Equilibrium*, Materials Research Society, Pittsburgh, 1998, p. 346.
- [25] R. Nitsche, M. Winterer, H. Halm, *Nanostruct. Mater.* 6 (1995) 679.
- [26] R. Nitsche, M. Winterer, M. Croft, H. Hahn, *Nucl. Instrum. Methods Phys. Res. B* 97 (1995) 127.
- [27] R. Winterer, R. Nitsche, S.A.T. Redfern, H. Schmahl, H. Hahn, *Nanostruct. Mater.* 6 (1995) 679.
- [28] R. Nitsche, M. Rodewald, G. Skandan, H. Fuess, H. Halm, *Nanostruct. Mater.* 7 (1996) 535.
- [29] G. Skandan, H. Halm, M. Roddy, W.R. Cannon, *J. Am. Ceram. Soc.* 77 (1994) 1706.
- [30] G. Skandan, *Nanostruct. Mater.* 5 (1995) 111.
- [31] S. Block, J.A.H. Da Jornada, G.J. Piermarini, *J. Am. Ceram. Soc.* 68 (1985) 497.
- [32] O. Ohtaka, T. Yamanaka, S. Kume, E. Ito, A. Navrotsky, *J. Am. Ceram. Soc.* 74 (1991) 505.
- [33] R.E. Cohen, M.J. Mehl, L.L. Boyer, *Phys. B* 150 (1988) 1.
- [34] A.P. Mirgorodsky, M.B. Smirnov, P.E. Quintard, *Phys. Rev. B* 55 (1997) 19.
- [35] A. Christiansen, E.A. Carter, *Phys. Rev. B* 58 (1998) 8050.
- [36] A. Tsoga, P. Nikolopoulos, *J. Mater. Sci.* 26 (1998) 5409.
- [37] W.W. Mullins, *J. Appl. Phys.* 59 (1986) 1341.